High intensity femtosecond laser deposition of diamond-like carbon thin films

F. Qian, V. Craciun,[a] and R. K. Singh
Department of Materials Science & Engineering, University of Florida, Gainesville, Florida 32611

S. D. Dutta and P. P. Pronko
Center for Ultrafast Optical Science, University of Michigan, Ann Arbor, Michigan 48109

(Received 28 January 1999; accepted for publication 11 May 1999)

Hydrogen-free diamond-like carbon (DLC) films have been deposited with a 100 fs (FWHM) Ti:sapphire laser beam at intensities I in the $10^{14}-10^{15}$ W/cm^2 range. The films were studied with scanning probe microscopy, variable angle spectroscopic ellipsometry, Raman spectroscopy, and electron energy loss spectroscopy. DLC films with good scratch resistance, excellent chemical inertness, and high optical transparency in the visible and near infrared range were deposited at room temperature. As the laser intensity was increased from 3×10^{14} to 6×10^{15} W/cm^2, the films showed an increased surface particle density, a decreased optical transparency (85%→60%), and Tauc band gap (1.4→0.8 eV), as well as a lower sp^3 content (60%→50%). The time-of-flight spectra recorded from the laser plume exhibited a double-peak distribution, with a high energy suprathermal ion peak preceding a slower thermal component. The most probable ion kinetic energy showed an $I^{0.55}$ dependence, increasing from 300 to 2000 eV, when the laser intensity was varied from 3×10^{14} to 6×10^{15} W/cm^2, while the kinetic energy of suprathermal ions increased from 3 to over 20 keV and showed an $I^{0.33}$ dependence. These high energy ions are believed to have originated from an electrostatic acceleration field established by suprathermal electrons which were formed by resonant absorption of the intense laser beams. [S0021-8979(99)07016-4]

I. INTRODUCTION

Ever since the invention of lasers, much attention has been directed at the understanding of the fundamentals of the laser–solid–plasma phenomena. The advances in laser plasma physics led to various practical applications in this area. In the field of materials science, the use of high intensity laser beams to deposit thin films has shown great promise in the synthesis of many advanced materials.[1] Pulsed laser deposition (PLD), known for well over 2 decades, has gained prominence in the deposition of a wide variety of thin film materials such as superconductors, semiconductors, dielectrics, metals, and biomaterials, among others.

The characteristics of PLD differ significantly from conventional thermal evaporation methods. PLD was first distinguished by the formation of high temperature (10^4-10^5 K) plasma, as well as ejected target species with high kinetic energies (~10s–1000s eV), followed by a forward-directed nature of the ablated materials. The energetic nature of laser induced plasma is believed to play an important role in synthesizing certain thermodynamically metastable materials, including diamond-like carbon (DLC), cubic silicon carbide (c-SiC), and cubic boron nitride (c-BN).[1]

DLC can be considered as a metastable form of carbon material covering the spectrum between diamond and graphite. But unlike crystalline graphite or diamond, which consists of 100% sp^2 and 100% sp^3, respectively, hybridized carbon atoms, DLC films have a mixture of sp^3 and sp^2 bonding and are generally amorphous, due to the lack of a long range. DLC possesses properties similar to those of diamond rather than graphite, including high mechanical hardness, high electrical resistivity, excellent chemical inertness, and optical transparency. In addition, a smoother surface topography, better adhesion to the underlying substrates, and relative ease in fabrication have made DLC films a desirable choice in certain applications. For these reasons, they have been one of the most actively researched thin film materials over the past 2 decades, primarily as an alternative to diamond coatings.

Most successful PLD depositions of DLC films conducted so far have employed either excimer (KrF, ArF, XeCl) or Q-switched solid state lasers such as various frequency modified Nd:YAG beams.[2–5] These lasers all have pulse duration in the nanosecond range. Depending on the laser energy and beam diameter focused on the target, laser intensities in the 10^8-10^{11} W/cm^2 range are most commonly achieved. Past experiments have indicated that the fraction of sp^3 bonds increased as a function of increasing laser intensity. The plasma formed under these conditions was found to consist of ionized carbon particles with moderately high kinetic energies, increasing from several eV up to several hundreds of eV as a function of laser intensity. Conversely, as a kinetic condensation process, formation of the metastable sp^3 bonding structure is expected to be destroyed under excessive high energy ion bombardment, resulting in the more stable sp^2 graphitic structure as recently shown.[5]

[a]Electronic mail: vcrac@mail.mse.ufl.edu

This motivated us to investigate the growth of DLC films using laser beams with a 100 fs (FWHM) pulse duration. The laser system employed in our study was a solid state Ti:sapphire laser system based on the chirped pulse amplification (CPA) technique, which enables the generation of high peak intensity laser pulses with extremely short pulse width.[6] By using this system, we were able to increase the intensity up to the $10^{14}-10^{15}\,W/cm^2$ range with only moderate laser energies. The laser plasma created under these conditions was studied through time-of-flight (TOF) experiments. This investigation was intended to establish a correlation between the ablated carbon ion kinetic energy and the grown DLC film properties, as a function of laser intensity.

II. EXPERIMENTS

DLC films were deposited using 100 fs Ti:sapphire pulses at laser intensities within the $3\times10^{14}-6\times10^{15}\,W/cm^2$ range. The pulse is near Gaussian shaped, centered at around 780 nm wavelength, with a FWHM of 100 fs. Due to compressor gratings absorption, the maximum laser energy is about 40 mJ.

The deposition system consists of a high vacuum deposition chamber coupled with vacuum laser beam delivery tubes (base pressure was maintained at 2×10^{-6} Torr). A high purity (>99.999%) polycrystalline graphite disk was used as the ablation target. The distance between the target and the substrate was kept at 4 cm during each deposition. A thin 3 mm MgF_2 laser window served as the front vacuum window. A *p*-polarized, high damage threshold reflective mirror positioned inside a turning box directs the beam into the deposition chamber. A gold plated aluminum off-axis parabolic mirror was used to focus the incoming laser beam onto the target. The parabolic mirror has a 10 cm effective focal length and a 60° off-axis angle.

The femtosecond laser beam was capable of breaking down air even at relatively low energy levels. During film deposition, the target was placed at an off-focal position to maintain a larger spot size. This was found to be necessary to keep the otherwise tightly focused beam from cutting a deep trench on the target surface. A minimum beam diameter of 50 μm was used in calculating the Ti:sapphire laser intensity in our study. This compares with a measured focal spot of 11 μm, using an image relay technique; at low laser intensities, a microscope lens was positioned near the mirror focal and it projected the image of the focal spot onto a charge-coupled device (CCD) camera. Conversely, a damaged surface spot with 80 μm in diameter was measured under an optical microscope.

The DLC films were deposited onto fused silica and silicon substrates at base vacuum pressure. The SiO_2 substrates were optically polished on both sides with a roughness <20 Å. Silicon substrates were single crystal wafers cut into 1 cm×1 cm squares, which were ultrasonically cleaned in acetone/methanol before been loaded into the deposition chamber. During the deposition processes, different intensity levels were achieved by varying the incident laser energy and the beam spot size, while keeping the laser pulse width constant. The deposition conditions for DLC films are summarized in Table I.

TABLE I. Experimental conditions for Ti:sapphire laser deposition of DLC films.

Laser source	Ti:sapphire (780 nm)
Repetition rate	10 Hz
Pulse width (FWHM)	100 fs
Target–substrate distance	4 cm
Minimum spot size	50 μm
Peak intensity	$3\times10^{14}-6\times10^{15}\,W/cm^2$
Substrate	Si, SiO_2
Substrate temperature	Room temperature

The film properties were analyzed with various techniques and correlated with the laser intensity. Carbon ion kinetic energy as a function of laser intensity was measured by TOF experiments. A field-free drift tube coupled with a Faraday ion collector was used for this.[7] Ion transit time between the target surface and the Faraday cup was measured as a function of laser intensity. The ion velocity was determined from the time lapse between the laser onset and the TOF distribution peak, which corresponds to the most probable carbon ion velocity V_m with a Boltzmann–Maxwellian-like distribution. Their kinetic energies can then be calculated from $KE=0.5MV_m^2$, where M is the carbon ion mass. Ion signals collected by the Faraday cup were monitored by a digital oscilloscope and relayed through a general purpose interface bus card to a computer. The triggering signal was provided by the Pockels cell wave voltage, which coincides with the onset of each laser pulse. The Faraday cup surface was kept perpendicular to the target normal for all the TOF measurements.

III. RESULTS AND DISCUSSION

This section details the experimental results of our investigation. First, results from the TOF experiments are presented. This is followed by a presentation of the DLC film properties analyzed by various techniques.

A. TOF measurements

TOF data were taken at base pressure and averaged over eight pulses on the oscilloscope, with laser intensity in the $1\times10^{14}-6\times10^{15}\,W/cm^2$ range. The upper intensity limit was typical of the maximum laser intensity used in making DLC films, while the lowest intensity value was determined by the oscilloscope signal/noise ratio.

Figure 1 shows a typical TOF spectrum taken at a laser intensity of $3\times10^{14}\,W/cm^2$. The ''zero time,'' corresponding to the moment the laser pulse strikes the target surface, is referenced by the early spike on the spectrum preceding the main plasma peak, which was generated by the soft x rays emitted by the plasma. Notice that in addition to the main ion peak marked as V_m, there is a second peak marked as V_s in the spectrum, preceding the main peak. When converted into ion velocity (see Fig. 2), this early peak represents a component of the carbon plasma expanding at a much faster speed V_s than that of the most probable ion velocity V_m. At this intensity level, V_m was calculated to be around 6×10^6

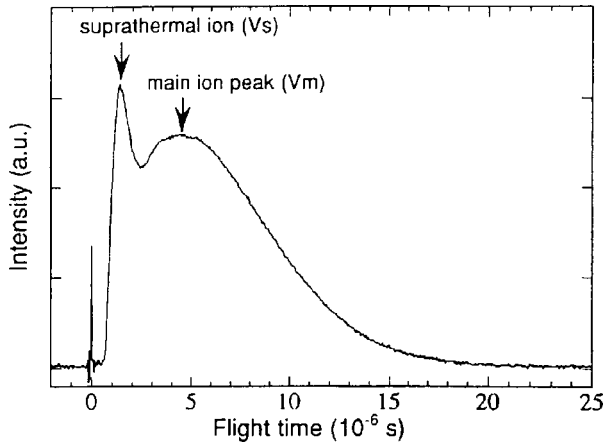

FIG. 1. TOF spectrum plotted on the time scale at a laser intensity of 3×10^{14} W/cm^2.

cm/s, corresponding to a carbon ion kinetic energy E_m of approximately 250 eV. On the other hand, V_s was estimated to have a value of 2.4×10^7 cm/s, corresponding to an ion kinetic energy E_s on the order of 3.5 keV.

We designated the carbon ions responsible for the early peak as ''suprathermal ions.'' Here the term ''suprathermal'' is a relative one used with respect to the main ion peak, which itself may have a kinetic energy much higher than that represented by the plasma thermal energy. Both the main and suprathermal plasma peaks shifted to shorter time scales at higher laser intensities. The carbon ion velocities V_m and V_s were computed and plotted in Fig. 3 as a function of laser intensity. Assuming atomic carbon ions, their kinetic energies, E_m and E_s, were calculated and shown in Fig. 4. The most probable carbon ion kinetic energy E_m had a maximum value of ~2.0 keV at a laser intensity of 6×10^{15} W/cm^2. The suprathermal ion kinetic energy E_s is, however, at least one order of magnitude higher than E_m at each measured intensity level. E_s reached a maximum value of ~25 keV at 6×10^{15} W/cm^2. Data fitting yielded $E_m \propto I^{0.55}$ and $E_s \propto I^{0.33}$, I being the laser intensity.

The observation of suprathermal ions in a femtosecond laser induced plasma has not been previously reported. Although the suprathermal ions constitute only a small fraction of the total ionized particles generated in the laser plume, they could nonetheless play a significant role in the formation of metastable DLC film structures. If the optimal ion kinetic energy of laser induced plasma does indeed fall between several tens to several hundreds of eV as suggested by earlier experiments and clearly shown recently for nanosecond laser pulses by Merkulov *et al.*,[5] these suprathermal ions alone could very well push the resultant films over the potential barrier back into the graphitic regime.[8] Although the neutral carbon atoms are known to form the major part of the plasma plume at latter stages, their kinetic energy is too small in comparison with that of ions and suprathermal ions and their role in changing the film structure and composition is marginal. We believe that the suprathermal ion peak detected in the TOF spectra arises from highly charged carbon ions, as suggested earlier by Ehler[9] and Stevefelt and Collins.[10] We were unable to derive the exact ion charge state with our present setup. An electrostatic spherical sector analyzer, which will be able to distinguish ions with different mass/charge ratios, is currently under construction.

The mechanism of suprathermal ion formation should be related to the generation of suprathermal electrons and the electrostatic field established by these electrons. At laser intensities of 10^{14} W/cm^2 and above, a plasma absorption mechanism called resonant absorption, may play a more important role than the inverse bremsstralung absorption

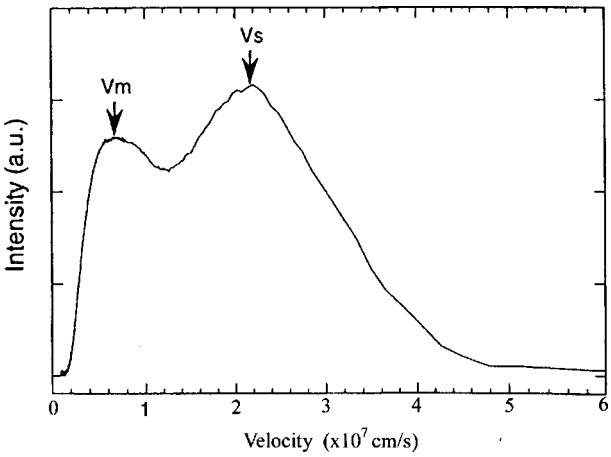

FIG. 2. TOF spectrum plotted on the velocity scale at a laser intensity of 3×10^{14} W/cm^2.

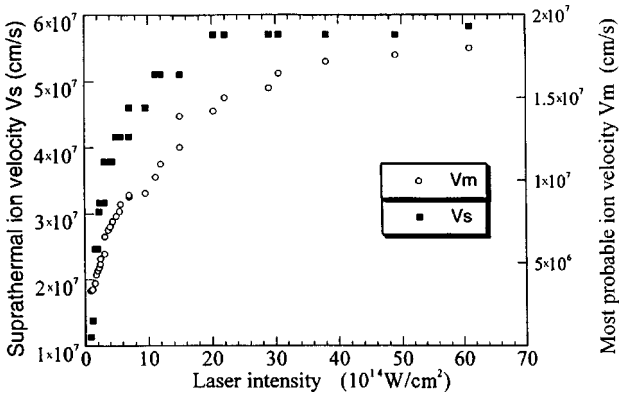

FIG. 3. Most probable and suprathermal carbon ion velocity plotted as a function of laser intensity.

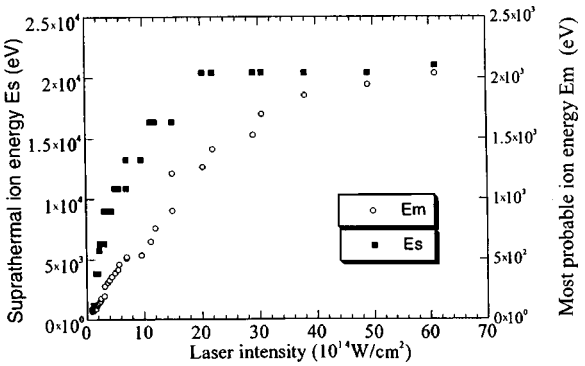

FIG. 4. Most probable and suprathermal carbon ion kinetic energy plotted as a function of laser intensity.

mechanism. At these high laser intensities, when a Ti:sapphire laser beam is incident on the graphite target at an oblique angle of 60° off the parabolic mirror, the laser wave will be refracted by the charge density gradient with a turning point at $n=n_c\cos^2(60°)=4.5\times10^{20}/\mathrm{cm}^3$, before the critical density surface. For a *p*-polarized laser beam such as the one used here, where the laser electric field vector is parallel to the plane of incidence, the solution of Maxwell's equation showed a singularity in the magnitude of the oscillating electric field vector at the point of reflection. The oscillating field can resonantly drive an electron plasma wave to very large amplitudes. This resonant singularity may be viewed as a tunneling of the evanescent wave from the turning point to the critical layer, where it resonantly excites a plasma.[11] As a result, oscillatory motion of the electrons due to this abnormally high electric field creates a charge separation, which at a finite electron temperature leads to the propagation of a plasma wave. At finite temperature there is a direct transfer of energy from photons to plasma wave which subsequently converts its energy to electron thermal energy. This collisionless wavebreaking process in resonance absorption gives rise to the so-called suprathermal electrons.

Suprathermal electrons have been previously observed in laser fusion studies,[12–15] where the laser intensities used are similar to those generated by the femtosecond pulses in our experiment. These suprathermal or sometimes termed ''fast electrons'' are characterized by a temperature that is on the order of 10–20 times higher than that of the background plasma temperature and scales as $(I\lambda^2)^aT^b$, where *a* and *b* generally have values between 0.25 and 0.50 and *I* is the laser intensity, λ is the laser wavelength, and *T* is the background plasma temperature. Particle simulations by Freidberg *et al.*[16] also showed that a small number of suprathermal electrons could be created as an outward moving stream originating from the critical density region.

Due to their small inertia, the plasma electrons will start to move towards the vacuum side once the laser pulse terminates and the balancing ponderomotive pressure no longer acts as an impeding force against the thermal pressure. The much heavier carbon ions, however, will remain relatively ''cold'' and stationary during the pulse span. In this early stage of plasma expansion, with an electron density on the order of $10^{23}/\mathrm{cm}^3$, the plasma has a Debye length $\lambda_D=740(T_e/n_e)^{0.5}$ (in cgs units) of the order of only several angstroms. The ions thereby will not be able to feel the effect of the electric field established by the electrons and no ion acceleration occurs until the plasma has expanded to a much lower density level, where the Debye length becomes comparable to the plasma dimensions. The requirement for the plasma as a whole to maintain quasineutrality then establishes a time dependent electrostatic potential in the lower density coronal region. Here the suprathermal electrons lead the expansion of the plasma and, through the radial electric field set up by charge separation, a fraction of the plasma ions will be accelerated to high velocities according to their charge *Z*. We believe it is this process that produced the suprathermal ions observed in our TOF experiments.[17,18] In the meantime, a return electron current is established by this electric field to maintain both charge and momentum balances.[19] These ions will eventually move at the same velocity as the suprathermal electrons, and their kinetic energy saturates when all the electron energy has been extracted.

A quantitative measurement of the suprathermal ion fraction is difficult. This is because the TOF peaks corresponding to suprathermal and to slow ions are a function of both the particle number and their charge state, which could not be differentiated with the current setup. However, if one assumes that ions have the same charge and both assume Maxwellian-like distributions, it can be estimated that at a laser intensity of $3\times10^{14}\,\mathrm{W/cm}^2$, their ratio is $\sim10^{-2}$, and it decreases to $\sim10^{-3}$ at $6\times10^{15}\,\mathrm{W/cm}^2$. This finding is not well explained and we suspect that the contrast ratio of the Ti:sapphire laser pulse may have played a role.

There are two factors affecting the contrast ratio in a CPA laser system. One is the so-called amplified spontaneous emission (ASE) which originates from spontaneous emission from various amplifier stages. ASE is present as a low but rather broad background noise with a time scale up to tens of nanoseconds in the output spectrum. The second factor involves the stretching/compression scheme of the laser system. When there is a compressor/stretcher mismatch and/or spectral distortion by the amplifier system, the compressed laser pulse may have pedestals, or ''wings'' in front of and after the main peak, which can extend to over hundreds of picoseconds. For a subpicosecond Ti:sapphire laser pulse with extremely high intensity, even a relatively small amount of prepulse can generate a low density plasma on the target surface before the main laser peak arrives. Assuming background ASE/pedestals with time scales on the order of 1 ns, a minimum contrast ratio of 10^6:1 would be required to eliminate the possibility of a preplasma formation on the graphite target, even at the lowest laser intensity of about $1\times10^{14}\,\mathrm{W/cm}^2$ employed in our study. This is because the ablation threshold for graphite for a ns pulse duration was estimated to be around $1\times10^8\,\mathrm{W/cm}^2$.[20] Therefore, when the laser intensity is increased to higher values, it is very likely that a low density plasma may have been created before the arrival of the femtosecond pulse. As a result, these less intense, long duration prepulses will generate more ''slow ions'' in the plasma. They may obscure the TOF signal from the suprathermal, or ''fast ions'' induced by the main femtosecond pulse, thus making a quantitative estimation of the suprathermal ion fraction unreliable.

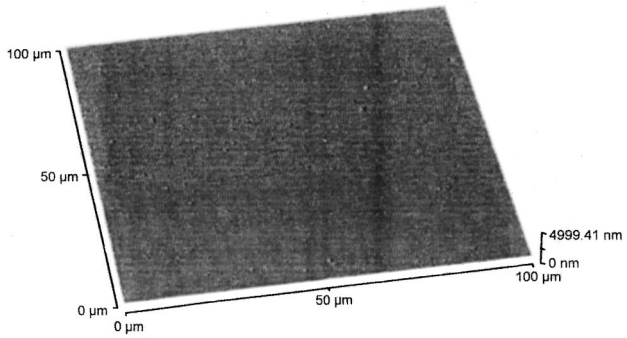

FIG. 5. AFM image of DLC film deposited by a Ti:sapphire laser at $3\times10^{14}\,\mathrm{W/cm}^2$.

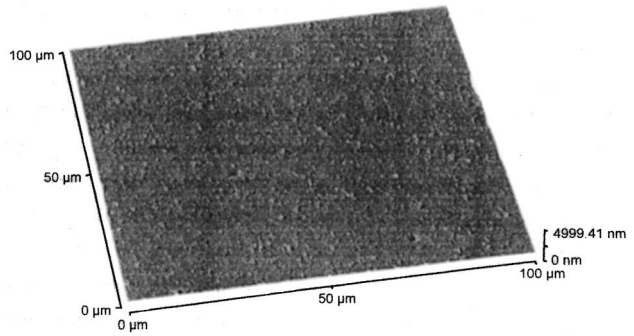

FIG. 6. AFM image of DLC film deposited by a Ti:sapphire laser at 1×10^{15} W/cm^2.

B. DLC film properties

1. Scanning probe microscopy (SPM)

The DLC films deposited on SiO_2 substrates are visually smooth and largely transparent with a light yellowish tint. Those deposited at higher intensities appear to be more absorbing with a darker appearance. The DLC films deposited onto Si substrates have a black and sometimes bluish tint. Color interference fringes can be seen on thinner samples. The films are resistant to the razor blade scratch test. They also remain intact after being submerged in a 1:3 HCl:HNO_3 solution for over 12 h, suggesting good chemical inertness. Thicker films, however, tend to buckle and peel off from the substrates once they are removed from the vacuum environment.

A TopoMetrix® 2000 series SPM, operated in the force sensor mode by applying a constant force on the sensor probe, also called an atomic force microscope (AFM) was used to study the film topography. Figures 5, 6, and 7 display the AFM images of DLC films deposited on SiO_2 at laser intensities of 3×10^{14}, 1×10^{15}, and 6×10^{15} W/cm^2, respectively. Under AFM, these films appeared to have high particle densities, especially for those grown at higher laser intensities, when the entire surface area was covered with micron-sized particles. The average particle size, however, remained largely unchanged. No large chunks of clustered particles were observed even on samples deposited at the highest intensity. Splashing of the target microparticles was visually observed in the laser plume, when tight focal spots were used.

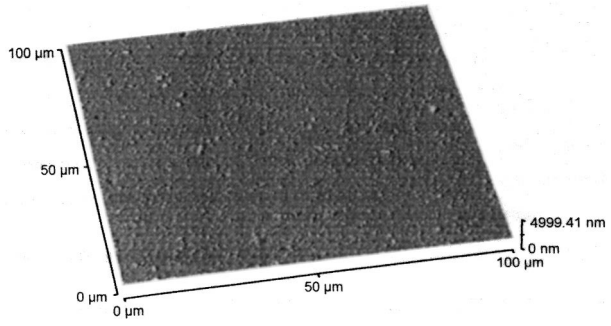

FIG. 7. AFM image of DLC film deposited by a Ti:sapphire laser at 6×10^{15} W/cm^2.

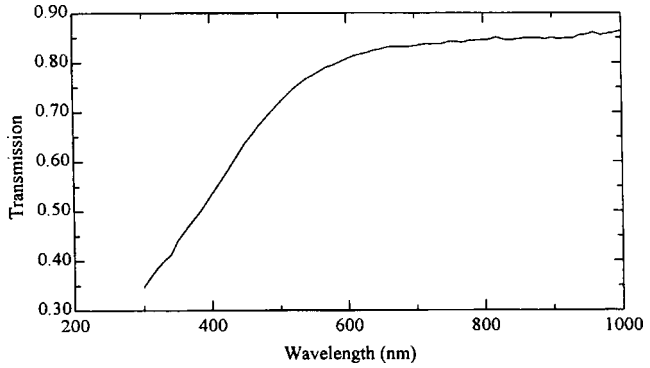

FIG. 8. Transmittance of DLC film deposited by a Ti:sapphire laser at 3×10^{14} W/cm^2.

2. Variable angle spectroscopic ellipsometry (VASE)

The optical properties of the DLC films deposited on SiO_2 substrates, n and k, the real and imaginary part of the film complex index of refraction, were analyzed by VASE ellipsometry (J. A. Woollam Company).

The n and k were measured as a function of the incident beam wavelength λ (300–1000 nm) as well as the angle of incidence ϕ (65° and 75°). To prevent the probe light reflected by the substrate backside from reaching the detector and interfering with the signal, we used fused silica substrates with a thickness of 3 mm. To obtain unique solutions for both the film thickness and its optical constants, the data obtained by VASE were correlated with the transmission data from the same sample.[21]

Intensity transmittance measurements were carried out by setting the ellipsometer in the straight through configuration ($\phi=90°$). A baseline intensity of the incident beam was first measured without the sample in place. The DLC film transmittance was then obtained by measuring the beam intensity with the sample in place and dividing the transmitted intensity by the baseline intensity. Plotted in Figs. 8 and 9 as a function of wavelength, are the transmittance of DLC samples deposited at laser intensities of 3×10^{14} and 6×10^{15} W/cm^2, respectively. The DLC film deposited at 3×10^{14} W/cm^2 has an optical transparency up to 85% in the IR region. It is also largely transparent in the visible spectrum down to about 600 nm and becomes more absorbing in

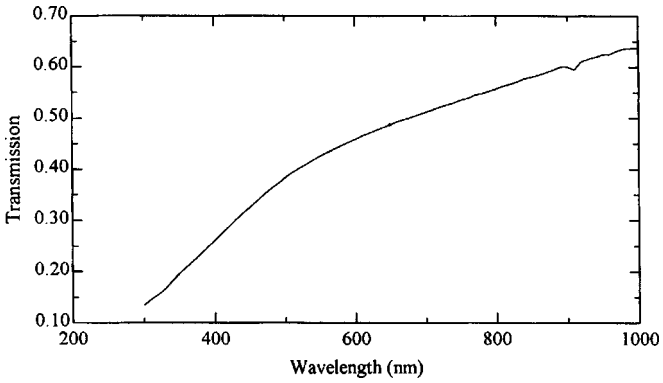

FIG. 9. Transmittance of DLC film deposited by a Ti:sapphire laser at 6×10^{15} W/cm^2.

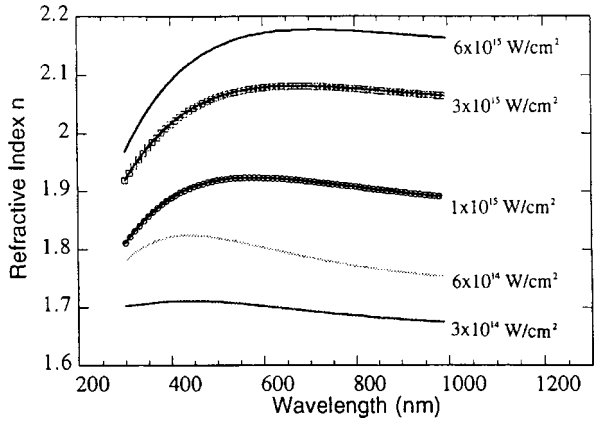

FIG. 10. Refractive index n of DLC films deposited by a Ti:sapphire laser, as a function of wavelength.

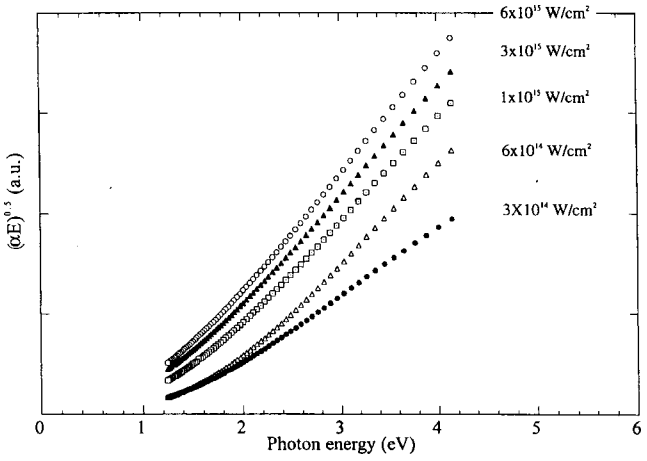

FIG. 12. Tauc plot of DLC films deposited by a Ti:sapphire laser.

the UV range. The film deposited at $6\times10^{15}\,\mathrm{W/cm^2}$, on the other hand, is much more absorbing with a 65% transparency at 1000 nm wavelength. At 600 nm, its transmittance is only about half that of the film deposited at $3\times10^{14}\,\mathrm{W/cm^2}$.

The best fits of the ellipsometric data were achieved with a parametric semiconductor model. The refractive index n and the extinction coefficient k of the DLC films are plotted in Figs. 10 and 11, 12 respectively, as a function of laser intensity. A rather consistent trend is seen among these DLC samples. As the laser intensity increases, the films become more absorbing (higher k) and refractive, consistent with the transmittance measurement. For each sample, the film is more transparent in the IR and visible range than in the UV region. Demichelis *et al.*[22] have demonstrated that it is possible to directly deduce the sp^3/sp^2 ratio of the DLC films from the experimental values of the complex dielectric constants ϵ_1 and ϵ_2. However, their approach could not be successfully carried out in our ellipsometry study since the maximum photon energy attainable was only about 4 eV.

Depending on film thickness and laser intensity, these DLC films were measured to have electrical resistance ranging from several hundred thousand to several mega-ohms. For amorphous semiconducting materials such as DLC films, the Tauc model[23] is often used to describe their optical band gaps, where the energy dependency of the absorption coefficient α is expressed as:

$$\alpha(E)=\frac{B(E-E_T)^2}{E}, \tag{1}$$

where E is the photon energy, B is a constant, and E_T is the Tauc band gap. The absorption coefficient α is calculated from $\alpha=4\pi k/\lambda$, where k is the extinction coefficient and λ is the photon wavelength. Table II summarizes the films thickness and Tauc band gap of DLC films deposited at laser intensities between 3×10^{14} and $6\times10^{15}\,\mathrm{W/cm^2}$.

As shown in Table II, the DLC films have Tauc band gaps ranging from about 1.5 to 0.8 eV, decreasing as a function of increasing laser intensity. The presence of an optical band gap in amorphous DLC films is significant. The graphite target, with 100% sp^2 bonds, is in effect a zero band gap semiconductor. On the other hand, a single crystal diamond with 100% sp^3 bonds has an optical band gap of 5.4 eV. It seems that diamond-like carbon, with its mixed sp^3 and sp^2 bonding structure, would have a higher band gap as the sp^3 bonding content increases. However, the assumption that there exists a simple linearity relationship between the film optical band gap and its sp^3 content is often false, because the optical band gap of DLC depends not only on the relative amount of sp^3/sp^2 bonds, but also on their distribution in the film structure. Robertson and O'Reilly[24] have shown that the mere presence of sp^3 sites in amorphous diamond-like carbons was not sufficient to produce an optical band gap. Instead, the sp^2 sites must be spatially correlated to produce a band gap even in the presence of sp^3 sites.

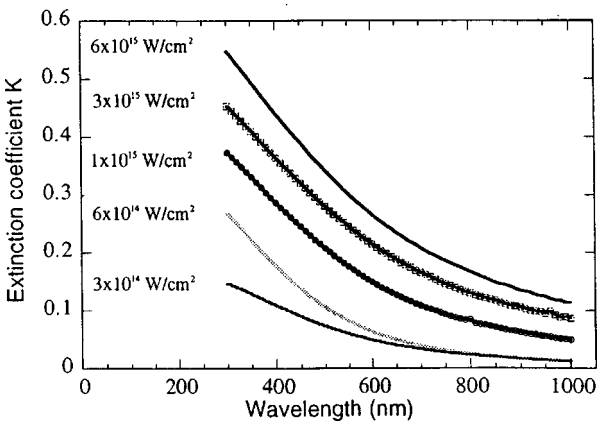

FIG. 11. Extinction coefficient k of DLC films deposited by a Ti:sapphire laser, as a function of wavelength.

TABLE II. Thickness and Tauc band gap of Ti:sapphire laser deposited DLC films.

Sample	Laser intensity ($\mathrm{W/cm^2}$)	Thickness (Å)	Tauc band gap (eV)
Femto-A	3×10^{14}	1506±10	1.5
Femto-B	6×10^{14}	1242±10	1.3
Femto-C	1×10^{15}	1350±10	1.1
Femto-D	3×10^{15}	811±10	1.0
Femto-E	6×10^{15}	853±10	0.8

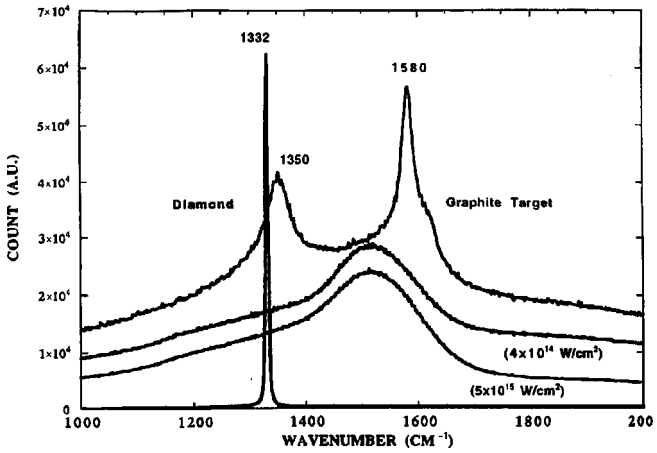

FIG. 13. Raman spectra of a typical DLC film, a graphite target, and a CVD diamond film.

For the Ti:sapphire laser deposited DLC films in our experiment, their band gaps showed a tendency to decrease as a function of increasing laser intensity. This can be related to the defect states introduced by the energetic carbon particles. It has been shown that there exists an inverse correlation between the defect density and the optical band gap of amorphous DLC films.[24] In a DLC film containing both π and σ bonds, the π defects are expected to be predominant due to their lower formation energy. A higher carbon ion kinetic energy will increase the amount of π defect states in the films, lowering the optical band gaps of films deposited at higher laser intensities. In the case of femtosecond laser deposited films, additional σ defects are likely to have been introduced because of the high energy suprathermal ion component found in the laser plasma, thus further decreasing the optical band gap.

3. Raman spectroscopy

Raman spectra were taken from the same DLC samples examined by ellipsometry. The instrument used is a Kaiser Optical System, Inc. HoloProbe spectrometer which consists of an imaging spectrograph integrated with a fiber–optic probe head, an Olympus BX60 microscope, a CCD camera, and various compact laser components. The laser source used in this spectrometer is a 532 nm diode-pumped, frequency-doubled Nd:YAG laser. The system's imaging spectrograph is equipped with a HoloPlex™ grating and placed in the axial-transmissive spectrograph configuration.[25] This compact design provides spectral coverage up to 4500 cm^{-1} in one single exposure.

The Raman spectra were taken with a laser power of 11 mW measured on the film surface. The probe beam diameter was determined to be ~16 μm with a 50× objective lens. The spectra acquisition time was set at 10 s. With the cosmic light filter on, actual acquisition time doubled to 20 s. Figure 13 shows typical Raman spectra taken from DLC samples deposited on SiO_2 substrates, along with those taken from a graphite target and a free standing CVD diamond film.

The Raman spectral features of the DLC films are distinctively different from that of the CVD diamond and the graphite target, as shown in Fig. 13. Instead of well-defined *D* and *G* peaks, these DLC samples exhibited a broadband structure covering the spectrum ranging from about 1000 to 2000 cm^{-1}. This broadband can be interpreted as a convolution of the two-component structure of a microcrystalline graphite: a relatively narrow *G* band centered at around 1550 cm^{-1} and a much broader *D* shoulder embedded at a lower wave number. A common practice in analyzing the small differences among these spectra is to mathematically fit them with two damped harmonic oscillator functions[26]

$$\frac{dI}{d\omega}=\frac{\Gamma\omega_0}{[(\omega_0^2-\omega^2)^2+4\Gamma\omega_0^2\omega^2]}, \tag{2}$$

where $dI/d\omega$ is proportional to the detector signal at ω, ω_0 is the undamped mode frequency, ω is the frequency shift from the laser line, and Γ is the damping constant. An integration of the above equation gives the intensity *I* associated with each Raman band. The Raman spectra were fitted in the spectral range between 1200 and 1800 cm^{-1}. Summarized in Table III are the parametric values used in fitting the Raman spectra, including the peak center position for the *G* and *D* bands, as well as their respective bandwidth.

When compared with the graphite target, the *G* band of every DLC sample was observed to have shifted from 1580 cm^{-1} down to the 1520–1530 cm^{-1} range. As the laser intensity increased from 6×10^{14} to 6×10^{15} W/cm^2, the *G* bands showed a slight upward shift, but their bandwidths (FWHM) did not exhibit a well-defined trend and remained largely unchanged. On the other hand, the *D* bandwidths displayed a clear upward drift as a function of increasing laser intensity, their values more than doubled from 150 to 340 cm^{-1} as the laser intensity was increased from 6×10^{14} to 6×10^{15} W/cm^2. The *D* band center did not have a well-

TABLE III. Fitted Raman parameters of Ti:sapphire laser deposited DLC films.

		G band (cm^{-1})		*D* band (cm^{-1})	
Sample	Laser Intensity (W/cm^2)	Center	FWHM	Center	FWHM
Femto-A	3×10^{14} (fluorescence)	—	—	—	—
Femto-B	6×10^{14}	1520	181	1321	150
Femto-C	1×10^{15}	1527	177	1327	215
Femto-D	3×10^{15}	1528	185	1325	270
Femto-E	6×10^{15}	1530	183	1342	340
Accuracy	—	±1	±3	±5	±10

defined correlation with the laser intensity either, although it also appeared to have downshifted to lower wave numbers (1321–1343 cm^{-1}) when compared with that of the graphite *D* band at 1345 cm^{-1}. The relationship between the *D* band center position and that of the DLC structure is less well established. Although it has been suggested that there was a possible *D* band downshift as a result of increasing sp^3 content and/or bond-angle distortion,[26,27] this observation has been rebutted by recent experiments.[28]

The observed *G* band downshifting from that of the graphite target has confirmed the notion that there exists a certain amount of sp^3 bonds as well as a certain degree of bond-angle distortion in these DLC films. It is also tempting to suggest that the films deposited at lower laser intensities have higher sp^3 fractions, in light that their *G* bands are centered at lower wave numbers and they have higher optical band gaps measured by ellipsometry. However, one has to be cautious because the effects of sp^3 content and bond-angle disorder on the *G* band downshift may not be easily differentiated, considering the fact that the existence of bond-angle distortion and sp^3 bonds in a DLC film are often correlated. In addition, it has been demonstrated that Raman band shift could be introduced as a result of residual stresses in the DLC films.[29] Our TOF and ellipsometry measurements have indicated that the DLC films are condensed from carbon particles with very different kinetic energy and they have unequal film thickness, which could give rise to various compressive stresses at the film/substrate interface. This residual stress cannot be easily relaxed because of the rigid SiO_2 substrate. Thereby the Raman band shift resulting from the residual stress and that from the change of structure disorder in the films often could not be separable.

Another conclusion that can be drawn from the Raman study is that the DLC films grown at higher laser intensity levels have a higher degree of bond-angle distortion, most likely caused by the higher particle energies. This is consistent with the study of Enke,[30] who found a direct relationship between the *D* bandwidth and that of the film bond-angle distortion.

As mentioned earlier, the *D* band center position did not exhibit a clear correlation with the laser intensity. In addition to possible complications caused by the presence of residual stress, some artifacts associated with the fitting process such as the selection of the fitting range, background intensity treatment, and the choice of oscillating functions might have played a role. Thereby for DLC films, which do not have well-defined vibrational/translational peaks, Raman spectroscopy analysis can at best be treated as a semiquantitative technique.

Sinha *et al.*[31] also observed that DLC films made by different techniques and exhibiting very different sp^3/sp^2 ratios seemed to present rather similar Raman features. This can be explained by the fact that sp^2 bonds, with a Raman scattering cross section of 500×10^{-7} $cm^{-1}\,sr^{-1}$, are as much as 50 times stronger Raman scatters than the sp^3 bonds.[32] As a result, the Raman spectrum will be most sensitive to the presence of sp^2 bonds in a DLC film, even when they only constitute a relatively small fraction of the total bonding sites.

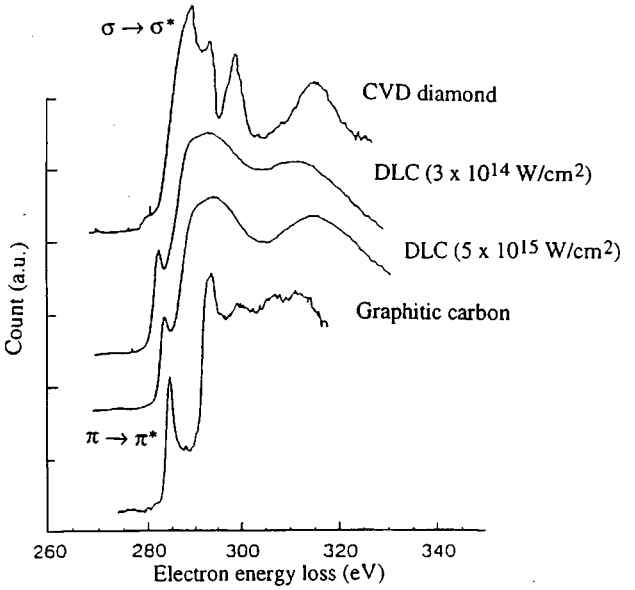

FIG. 14. *K*-shell edge EELS spectra of DLC films deposited by a Ti:sapphire laser at 3×10^{14} and 5×10^{15} W/cm^2, and along with that of a CVD diamond and a graphite film.

4. Electron energy loss spectroscopy (EELS)

EELS was used in this study to quantify the sp^3 content of the grown DLC films. A Gatan EELS with a maximum resolution of ~0.5 eV, defined by the FWHM of the zero loss peak, attached as an auxiliary to a field-emission analytical TEM, was used in our experiment. Carbon *K*-shell edge spectra were taken between 280 and 320 eV at an accelerating voltage of 150 kV. EELS samples were prepared by first depositing DLC films onto cleaved sodium chloride (NaCl) crystals, which were then floated off in de-ionized water onto copper grids. Film thickness was controlled to be less than 700 Å to alleviate the effects of multiple electron scattering.

Two DLC samples deposited at laser intensities of 3×10^{14} and 5×10^{15} W/cm^2, respectively, by the femtosecond Ti:sapphire pulses were analyzed by EELS. Figure 14 shows the *K*-shell edge EELS spectra acquired from these two DLC films. The EELS spectra of an arc evaporated carbon film and a free standing CVD diamond film, presumed to contain 100% sp^2 and 100% sp^3 carbon bonds, respectively, were used as standards and are also plotted in the same graph for comparison. All presented data were collected in one session to minimize the uncertainties caused by different probing conditions.

One can notice in Fig. 14 that transitions from the carbon 1*s* core level to the empty π^* antibonding states ($\pi\rightarrow\pi^*$ transitions) caused a strong absorption peak at ~285.5 eV for the graphitic carbon film, as a result of its local sp^2 bonding structure. On the other hand, the $\pi\rightarrow\pi^*$ peak is totally absent from the EELS spectrum taken from the CVD diamond film. This is because the sp^3 bonds in diamond contain only σ but no π orbitals. Instead, the $1s\rightarrow\sigma^*$, or $\sigma\rightarrow\sigma^*$ transitions (transitions from the 1*s* core level to the σ^* antibonding states) start at a higher energy of about 290 eV. These transitions also lead to distinct near-edge features

beyond 290 eV. This extended energy-loss fine structure is analogous to the extended absorption fine structure in x-ray absorption spectroscopy. In comparison, the EELS spectra for the two DLC samples, which contain a mixture of sp^3 and sp^2 bonded carbon atoms, lie somewhere between that of the graphitic carbon and the CVD diamond. The small $\pi \rightarrow \pi^*$ peaks measured in their EELS spectra suggest their diamond-like nature. In addition, due to the amorphous nature of these DLC films, the fine EELS features beyond 290 eV found in the diamond film have been lost.

Because the energy loss signal in a EELS spectrum is derived from primary electron interactions, the number of electrons that have lost energy due to $\pi \rightarrow \pi^*$ and $\sigma \rightarrow \sigma^*$ excitations can be directly estimated by the net integrated intensity of the corresponding peak in the *K*-shell edge region. A formula for estimating the sp^3 fraction can be expressed as[33]

$$\frac{sp^3}{sp^2} = \frac{N_\sigma - 3N_\pi}{4N_\pi} = \frac{(N_\sigma/N_\pi) - 3}{4}, \tag{3}$$

where

$$\frac{N_\sigma}{N_\pi} = 3\,\frac{(I_\pi/I_\sigma)_{\text{graphite}}}{(I_\pi/I_\sigma)_{\text{DLC}}}. \tag{4}$$

I_π and I_σ in Eq. (4) are the integrated area underneath the energy window 284–289 eV and 290–310 eV, respectively. N_σ/N_π is the ratio of the number of σ and π orbitals. It is numerically 3/1 for 100% sp^2 bonds, and 4/0 for 100% sp^3 bonds. Subscripts graphite and DLC in Eqs. (3) and (4) refer to the values obtained from the graphitic carbon film and the as-deposited DLC film, respectively. It has been estimated that the DLC film deposited at $3\times10^{14}\,\text{W/cm}^2$ has a sp^3 fraction of ~60%, and the one made at $5\times10^{15}\,\text{W/cm}^2$ has a sp^3 bonded carbon content of ~50%. The limiting factors in this estimation include possible bonding state change under the intense electron beam bombardment, as well as the uncertainties involved in background subtraction and integration window cutoffs.

IV. CONCLUSION

In summary, we have systematically experimented with the use of intense femtosecond laser beams to deposit thin, hydrogen-free diamond-like carbon film materials at laser intensities in the 10^{14}–$10^{15}\,\text{W/cm}^2$ range, which are at least three orders of magnitude higher than those employed by conventional PLD techniques, using a Ti:sapphire (100 fs at FWHM) laser beam.

The DLC film properties, including their surface topography, optical constants, bonding structure, as well as sp^3 content, were studied as a function of laser intensity. DLC films were grown at room temperature with good scratch resistance, excellent chemical inertness, and high optical transparency in the visible and near IR range. Film quality was observed to have decreased as the laser intensity was increased from 3×10^{14} to $6\times10^{15}\,\text{W/cm}^2$. This was evident by an increased surface particle density, a decreased optical transparency, and Tauc band gap, as well as a lower tetrahedrally bonded sp^3 carbon atom percentage.

The formation of laser deposited DLC films is believed to be an ion assisted energetic condensation process, with the carbon particle kinetic energy being one of most important factors affecting the film properties. For the femtosecond laser induced plasmas, the TOF spectra of carbon ions exhibited a double-peak distribution, with a fast moving suprathermal ion component preceding a majority of slower thermal ions. By varying the laser intensity in the 1×10^{14}–$6\times10^{15}\,\text{W/cm}^2$ range, it was estimated that the most probable ion kinetic energy displayed an $I^{0.55}$ dependence, increasing from 60 to over 2000 eV. On the other hand, the suprathermal ions were measured to have kinetic energies ranging from 3 to over 20 keV and a $I^{0.33}$ dependence. Only a small fraction of the carbon particles were made of suprathermal ions. They are believed to be generated by a time dependent electrostatic acceleration field induced by the suprathermal electrons which are formed due to resonant absorption of the intense, *p*-polarized laser beam. Because of their excessive energy, the highly energetic suprathermal ions in the femtosecond plasma are detrimental to the DLC film formation.

[1] *Pulsed Laser Deposition of Thin Films*, edited by D. B. Chrisey and G. K. Hubler (Wiley, New York, 1994).
[2] C. L. Marquart, R. T. Williams, and D. J. Nagel, Mater. Res. Soc. Symp. Proc. **38**, 325 (1985).
[3] W. Pompe, H. J. Scheibe, A. Richeter, H. D. Baner, K. Bewilogua, and C. Weissmantel, Thin Solid Films **144**, 77 (1986).
[4] C. B. Collins, F. Davanloo, E. M. Juengerman, W. R. Osborn, and D. R. Jander, Appl. Phys. Lett. **54**, 216 (1989).
[5] V. I. Merkulov, D. H. Lowndes, G. E. Jellison, Jr., A. A. Puretzky, and D. B. Geohegan, Appl. Phys. Lett. **73**, 2591 (1998).
[6] D. Strickland and G. Mourou, Opt. Commun. **56**, 219 (1985).
[7] W. Demtröder and W. Jantz, Plasma Phys. **12**, 691 (1970).
[8] J. J. Cuomo, D. L. Pappas, J. Bruly, J. P. Doyle, and K. Saenger, J. Appl. Phys. **70**, 1706 (1991).
[9] A. W. Ehler, J. Appl. Phys. **46**, 2464 (1975).
[10] J. Stevefelt and C. B. Collins, J. Phys. D **24**, 2149 (1991).
[11] T. P. Hughes, *Laser-Plasma Interactions*, Proceedings of the Twentieth Scottish Universities Summer School in Physics, edited by R. A. Cairns and J. J. Sanderson (Edinburgh University Press, Edinburgh, 1980), pp. 1–90.
[12] D. V. Giovanielli, J. F. Kephart, and A. H. Williams, J. Appl. Phys. **47**, 2907 (1976).
[13] D. W. Forslund, J. M. Kindel, and K. Lee, Phys. Rev. Lett. **39**, 284 (1977).
[14] K. Estabrook and W. L. Kruer, Phys. Rev. Lett. **40**, 42 (1978).
[15] J. D. Hares, J. D. Kilkenny, M. H. Key, and J. G. Lunney, Phys. Rev. Lett. **42**, 1216 (1979).
[16] J. P. Freidberg, R. W. Mitchell, R. L. Morse, and L. I. Rudsinski, Phys. Rev. Lett. **28**, 795 (1972).
[17] R. L. Morse and C. W. Nielson, Phys. Fluids **16**, 909 (1973).
[18] E. J. Valeo and I. B. Bernstein, Phys. Fluids **19**, 1348 (1976).
[19] M. G. Haines, *Laser-Plasma Interactions*, Proceedings of the Twentieth Scottish Universities Summer School in Physics, edited by R. A. Cairns and J. J. Sanderson (Edinburgh University Press, Edinburgh, 1980), pp. 145–218.
[20] D. H. Reitze, H. Ahn, and M. C. Downer, Phys. Rev. B **45**, 2677 (1992).
[21] P. G. Synder, J. A. Woollam, S. A. Alterovitz, and B. Johs, J. Appl. Phys. **68**, 5925 (1990).
[22] F. Demichelis, C. F. Pirri, and A. Tagliaferro, Phys. Rev. B **45**, 14364 (1992).
[23] J. Tauc, *Amorphous and Liquid Semiconductors*, edited by J. Tauc (Plenum, London, 1974), pp. 159–220.
[24] J. Robertson and E. P. O'Reilly, Phys. Rev. B **35**, 2946 (1987).
[25] H. Owen, D. E. Battey, M. J. Pelletier, and J. B. Slater, Proc. SPIE **2406**, 260 (1995).
[26] R. O. Dillon, J. A. Woollam, and V. Katkanant, Phys. Rev. B **29**, 3482 (1984).
[27] D. Beeman, J. Silverman, R. Lynds, and M. R. Anderson, Phys. Rev. B

30, 870 (1984).
[28] F. Qian, Master's thesis, University of Florida, 1993.
[29] D. S. Knight and W. B. White, J. Mater. Res. **4**, 385 (1989).
[30] K. Enke, Thin Solid Films **80**, 227 (1981).
[31] K. Sinha, J. Menendez, O. F. Sankey, D. A. Johnson, W. J. Varhue, J. N. Kidder, P. W. Pastel, and W. Lanford, Appl. Phys. Lett. **60**, 562 (1992).
[32] N. Wada, P. J. Gaczi, and S. A. Solin, J. Non-Cryst. Solids **35/36**, 543 (1980).
[33] D. L. Pappas, K. L. Saenger, J. Bruley, W. Krakow, J. J. Cuomo, T. Gu, and R. W. Collins, J. Appl. Phys. **71**, 5675 (1992).